TÜBİTAK

Turkish Journal of Earth Sciences

http://journals.tubitak.gov.tr/earth/

Research Article

Turkish J Earth Sci
(2016) 25: 592-610
© TÜBİTAK
doi:10.3906/yer-1601-10

Clay mineralogy and geochemistry of three offshore wells in the southwestern Black Sea, northern Turkey: the effect of burial diagenesis on the conversion of smectite to illite

Yinal N. HUVAJ*, Warren D. HUFF
Department of Geology, University of Cincinnati, Cincinnati, Ohio, USA

Received: 14.01.2016 • **Accepted/Published Online:** 24.05.2016 • **Final Version:** 01.12.2016

Abstract: The conversion of smectite to illite has long been studied by numerous researchers because of its importance as a diagenetic metric. Interpreting the pressure, temperature, and age of the sequences in which this conversion occurs provides the possibility to identify the historical maturation parameters of hydrocarbon sources. The Black Sea Basin is known to be an area that can provide source rocks for oil and gas production. The purpose of this study was to determine the clay minerals and their abundances, to establish a stratigraphic correlation among three wells, which is useful to select specific stratigraphic horizons for hydrocarbon exploration, and to predict paleotemperature ranges in the wells by using the conversion of clay minerals. The determination of the clay mineralogy and chemical composition of the three wells in the Black Sea Basin was done by several methods of analysis. These methods include powder X-ray diffraction (XRD), X-ray fluorescence spectroscopy (XRF), and environmental scanning electron microscopy (ESEM). All 54 samples were processed by XRD and XRF and 6 representative samples were selected for ESEM analysis. Based on the XRD results, the clay minerals determined in the samples are illite, smectite, and mixed-layer illite/smectite (I/S), which are the most abundant minerals calculated by the method described in Underwood and Pickering, plus kaolinite and chlorite. The chemical results of major oxides acquired from XRF analyses show that the changes in Na_2O and K_2O, which are the main actors in the conversion of smectite to illite, do not gradually increase or decrease. Since the Black Sea Basin is considered a rift basin, the maximum temperature ranges of the conversion were calculated by considering the maximum and minimum depths of the samples. These temperature ranges are 111–154 °C, 147–208 °C, and 48–59 °C for Well-1, Well-2, and Well-3, respectively.

Key words: Black Sea, burial diagenesis, clay mineralogy, geochemistry, illite, smectite

1. Introduction

Studying the stratigraphy of the Black Sea Basin (Figure 1) and its associated clay minerals is important for hydrocarbon exploration. The basin has long been known to be an area that can provide source rocks for oil and gas production. Because of the high cost of geophysical exploration of offshore areas, clay mineralogical studies become even more important as an aid to understanding diagenetic and thermal conditions responsible for hydrocarbon generation. The clay mineralogy of the three wells drilled by the Turkish Petroleum Corporation (TPAO) has not been determined before. Determining the changes in clay minerals may provide useful information, such as the extent to which burial diagenesis versus primary detrital input most accurately reflects the nature of the depositional environment, and thus understanding such conditions will help geologists to make a connection between the temperature that allows the changes in clay minerals and the temperature of occurrence of hydrocarbon resources. Determining of changes in clay minerals and understanding the mechanism that causes to such changes can also be useful for petroleum companies for interpreting the source rock occurrence zones. For these reasons, studying the clay minerals in the Black Sea Basin area has become important in recent years.

Clay mineral analysis has been used as a tool in terms of predicting paleoenvironmental conditions, stratigraphic correlation, and hydrocarbon generation zone identification to determine target interval and diagenetic conditions of hydrocarbon-bearing formations since the 1950s (Weaver, 1958, 1960; Hower et al., 1976; Hoffman and Hower, 1979). Since then, clay minerals have been used to determine the hydrocarbon emplacement time and for petroleum system analysis (Yariv, 1976; Liewig et al., 1987; Hamilton et al., 1989; Kelly et al., 2000; Drits et al., 2002; Jiang, 2012).

The structure of smectite changes with increasing burial depth; then the mineral disappears under burial conditions and the possible mechanism is a beneficiation of degraded and fragmental mineral lattices by the gradual fixation

* Correspondence: huvajyn@mail.uc.edu

Figure 1. Tectonic settling of Turkey and Black Sea (slightly modified after Okay, 2008).

of potassium and magnesium to form illite and chlorite, respectively (Burst, 1959). In the Upper Cretaceous shale section in Cameroon, smectite is converted to illite with increasing depth of burial (Dunoyer de Segonzac, 1964). The conversion of smectite to illite depends on the effects of burial diagenesis (Perry and Hower, 1970); they concluded that there is a linear relationship between the increasing potassium content of the clay-size fraction and the decrease of expandability. Therefore, potassium availability is important in the transformation of smectite to illite. For example, during burial diagenesis potassium feldspar and/or mica decompose and potassium is released (Hower et al., 1976). Freed and Peacor (1992) expressed the view that the conversion of smectite to illite requires fixation of K in interlayer sites and this conversion is concomitant with the substitution of Al for Si in tetrahedral sites. Others (e.g., Fowler and Young, 2003) suggested that the conversion proceeds by means of dissolution of a smectite and reprecipitation as an illite.

2. Geological setting

The Black Sea is one of a number of ocean basins around the Tethyside orogenic belt (Görür, 1988). It is a remnant of the Tethys Ocean, which existed between the two megacontinents, Gondwana in the south and Laurasia in the north of today's Turkey (Okay et al., 1996; Okay, 2008). The area for this study hosts the three offshore wells in the southwest of Black Sea along the Turkish margin (Figure 1) and is located in the tectonic unit called the "İstanbul Zone", which is a part of the western Pontides region in northern Turkey, as described in Yılmaz et al. (1997), Okay and Tüysüz (1999), and Okay (2008). The İstanbul Zone was located in the Odessa shelf, today's Ukraine, between the Moesian platform and the Crimea until the

Lower Cretaceous. During the Aptian–Albian time in the late part of the Lower Cretaceous, approximately 120 Ma ago, it was rifted and started to move southward (Görür, 1988; Okay et al., 1994) and during the Early Eocene, the İstanbul Zone collided with the Sakarya Zone (Okay and Tüysüz, 1999).

The stratigraphic sequence of the İstanbul Zone (Figure 2) starts with a Precambrian crystalline basement (Okay et al., 1994, 1996; Okay and Tüysüz, 1999; Okay, 2008). This unit is characterized by gneiss, amphibolite, metavolcanic rocks, meta-ophiolite, and Precambrian-aged granitoids (Chen et al., 2002; Yigitbas et al., 2004; Ustaömer et al., 2005; Okay, 2008). This basement is unconformably overlain by a continuous, well-developed (Okay et al., 1996; Okay, 2008), and transgressive (Okay and Tüysüz, 1999) sedimentary sequence from Ordovician to Carboniferous in age. This sequence was folded and deformed during the Variscan/Hercynian orogeny in the Carboniferous (Okay et al., 1996; Okay and Tüysüz, 1999; Okay, 2008). Stratigraphically, the Paleozoic sequence of the İstanbul Zone shows different characteristics in the west and the east portions of the terrane. In the western part, Carboniferous units mainly consist of more than 2000 m of deep sea turbidites forming a sandstone/shale sequence,

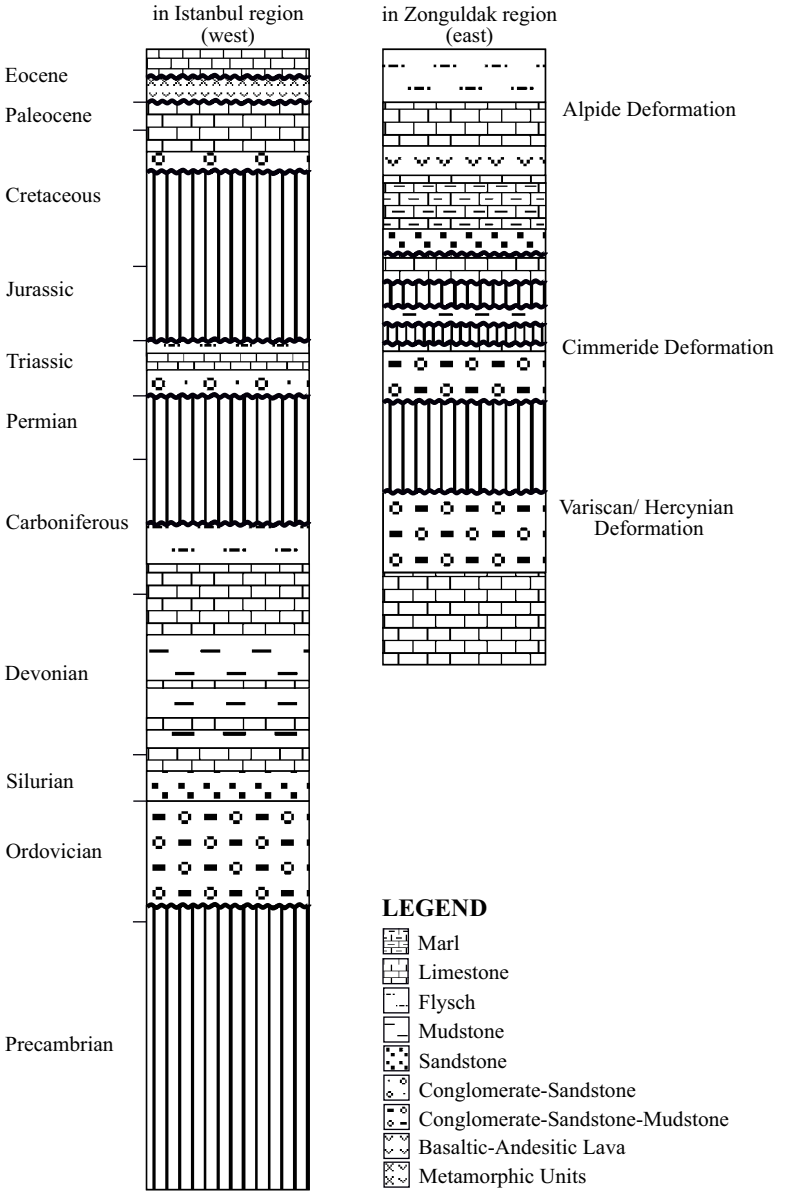

Figure 2. Illustration of stratigraphic sequence of İstanbul Zone (not to scale) (modified after Okay and Tüysüz, 1999).

and pelagic limestones with radiolarian cherts. The age of the limestones and cherts is Visean (Mississippian) of the Early Carboniferous and the age of the turbidites is Namurian (Pennsylvanian) of the Late Carboniferous. In the eastern part, however, the Carboniferous is characterized by Visean shallow marine carbonates and a Namurian and Westphalian (Pennsylvanian) paralic coal series (Okay and Tüysüz, 1999; Okay, 2008). Another difference between these two parts is that the Variscan/ Hercynian orogeny started earlier and was stronger in the western part than in the eastern one (Okay and Tüysüz, 1999). The Paleozoic sequence is unconformably overlain by the Triassic sedimentary sequence, which is well-developed in the east of the İstanbul Zone. This sequence shows a typical transgressive development, about 800 m thick. It starts with red sandstones and basaltic lava flows, continues with shallow marine marls, limestones, and then deep marine limestones, and ends with deep sea sandstones and shales. In the western part of the İstanbul Zone, the Jurassic and Lower Cretaceous rocks are absent, and the Triassic sequence is unconformably overlain by Upper Creataceous clastic rocks and limestones, and Eocene neritic limestones unconformably overlie the Mesozoic units. However, there are Middle Jurassic to Eocene rocks marked by small unconformities in the eastern part of the İstanbul Zone. The Jurassic flysch and Upper Cretaceous limestones, clastics, and marl units overlie to the Triassic rocks, and this sequence is overlain by Palaeocene and Eocene pelagic limestones and flysch (Okay and Tüysüz, 1999; Okay, 2008).

2.1. Geology of the three offshore wells

Based on the privacy policy of the Turkish Petroleum Corporation, the names of the wells have been numbered and symbolized, and formation names also symbolized.

The samples acquired from the Turkish Petroleum Corporation are mostly from the KS formation. All samples of Well-2 (Well "KC") and Well-3 (Well "A") are from the KS formation, two samples of Well-1 (Well "I") are from the GR formation, and one sample is from the AKV formation. Samples of Well-1 and Well-2 have been selected from marl units that show slightly different characteristics such as color and clay content. Nine of the twelve samples of Well-3 have been selected from mudstone, one sample of the Well-2 is from claystone, and the others are from marl lithologies.

Well-1 was drilled in the Black Sea near the western border of the Central Pontides tectonic unit of Turkey. This location is approximately 25 km from the eastern boundary of the İstanbul Zone (Figure 3).

Nineteen samples were selected from Well-1 (Figure 4). Well-2 is located approximately 60 km west of Well-1 and is represented by 23 samples (Figure 5). Twelve samples have been received from Well-3 (Figure 6). This well is located approximately 320 km west of Well-2.

3. Materials and methods

All 54 cutting samples were provided by the Turkish Petroleum Corporation Research Center and the samples were hand-picked to ensure representative lithology or different characteristics of the same lithology at different depths. A Siemens D-500 X-ray diffractometer using Cu-Kα radiation was used to obtain XRD patterns of the samples (Figure 7). All samples were prepared by using the smear mount method described by Moore and Reynolds (1997). The particle size of the analyzed materials is <2 μm and this particle size has been achieved by following the particle size separation methods described also by Moore and Reynolds (1997).

Chemical analyses were performed with a Rigaku 3070 wavelength-dispersive X-ray fluorescence spectrometer. Samples were finely ground in a tungsten carbide ball mill canister for 7–8 min. After this grinding process sample grains became less than 5 μm in size, which is an appropriate size to prepare XRF pellets. The powdered sample was then compressed into thin pellets using the Spex 3624B X-Press machine. Prepared XRF pellets were placed into a 55 °C oven for 24 h until analyzed.

A number of different types of grains such as apatite, biotite, and quartz phenocrysts were photographed and chemically analyzed with a Phillips XL-30 field emission gun (FEG) environmental scanning electron microscope (Figure 8). Each cutting sample was sieved through a No. 100 sieve (0.15 mm/0.059 in) to remove coarse grains and a No. 200 sieve (0.075 mm/0.029 in) to remove clay-sized particles. During the sieving processes cutting samples were washed with water and after sieving they were left in a 60 °C oven for drying. After they dried, individual grains were handpicked under the microscope and stuck onto the adhesive surface of an ESEM sample holder by using a special fiber.

4. Results and discussion

Based on the XRD patterns, the clay minerals determined in the samples are illite, smectite, mixed-layer illite/smectite (I/S), kaolinite, and chlorite. The percentages of these minerals were calculated by using the method described in Underwood and Pickering (1996). According to the calculations, illite is the dominant mineral in all three wells. The average illite percentages are 51%, 51%, and 46% in Well-1, Well-2, and Well-3, respectively. Smectite is the second most abundant mineral as 25%, 19%, and 18% in Well-1, Well-2, and Well-3, respectively (Figure 9). On the other hand, as can be seen in the XRD patterns there is a mixed-layer illite/smectite (I/S) phase in almost all samples. However, the I/S phase is not dominant and individual illite and smectite minerals also exist independently from the mixed-layer phase. This unusual character of I/S has not been discussed widely in many papers before. As

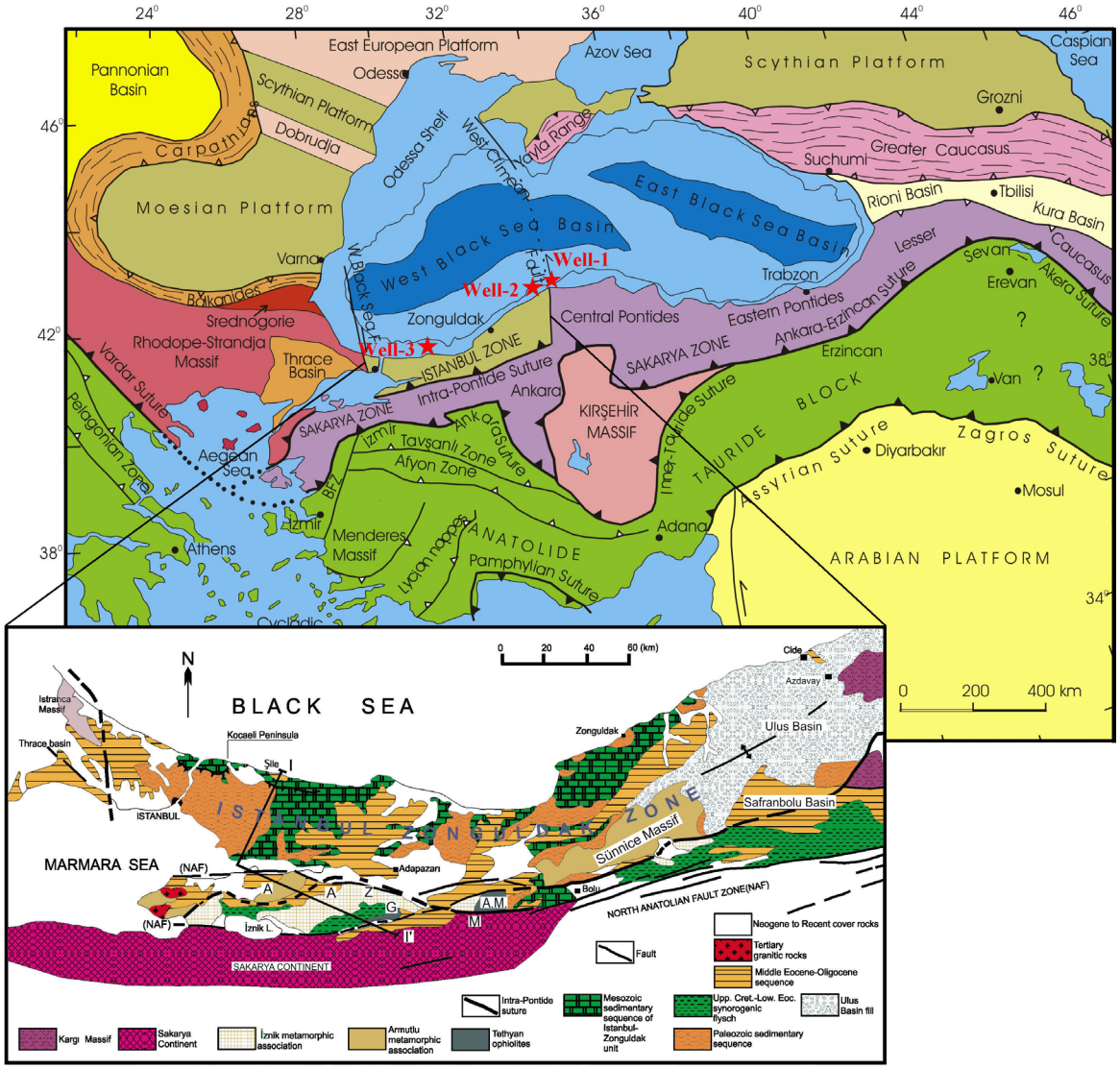

Figure 3. Location map of the three offshore wells on the tectonic unit map of Turkey (close-up view of the red-lined rectangular area in Figure 1) (slightly modified from Okay and Tüysüz, 1999; and Yilmaz et al., 1997).

discussed in Moore and Reynolds (1997), the existence of the I/S in the air-dried XRD pattern causes a slight shifting on the illite 002 peak position in the glycolated pattern. In our samples, there is no such a shifting effect after glycol treatment. It demonstrates that the I/S phase in our samples is not dominant, and the dominant phases are discrete illite and smectite. Based on the clay mineral assemblage and percentages discussed above, it can be concluded that the samples contain both detritic primary illite as individual phases and diagenetic (or neoformative) illite as mixed-layer illite/smectite phases. This conclusion is supported by the graphics of illite crystallinity (Kübler index (KI)) measurements shown in Figure 10. These measurements have been obtained by using the method described in Jaboyedoff et al. (2001). As is known, the KI is used for understanding the degree of diagenesis and low-grade metamorphism (Jaboyedoff et al., 2001). As discussed in Kübler (1967), the epizone–anchizone boundary was defined at 0.25 $\Delta 2\theta$ CuKα, and the anchizone–diagenesis boundary was defined at 0.42 $\Delta 2\theta$ CuKα. The KI values of many of the samples are in the epizone and anchizone and the values of some of the samples are in the diagenetic zone. In Well-1 two samples do not give a KI value, because these samples are from the faulted/thrust zones. Based on the KI interpretation, the mixed-layer I/S formation has started in each well. However, the unusual patterns (sharp fluctuations) of the KI graphics may be caused by the existence of the diagenetic and detritic forms of illite together.

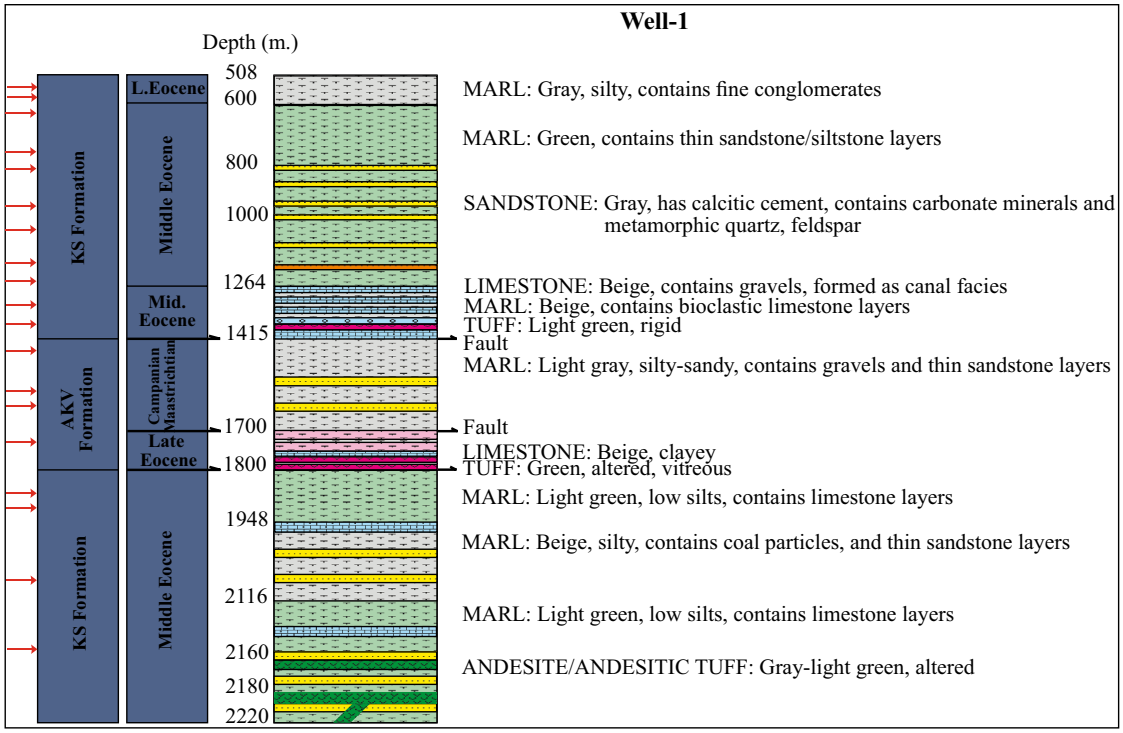

Figure 4. Illustration of columnar section of Well-1 (not to scale).

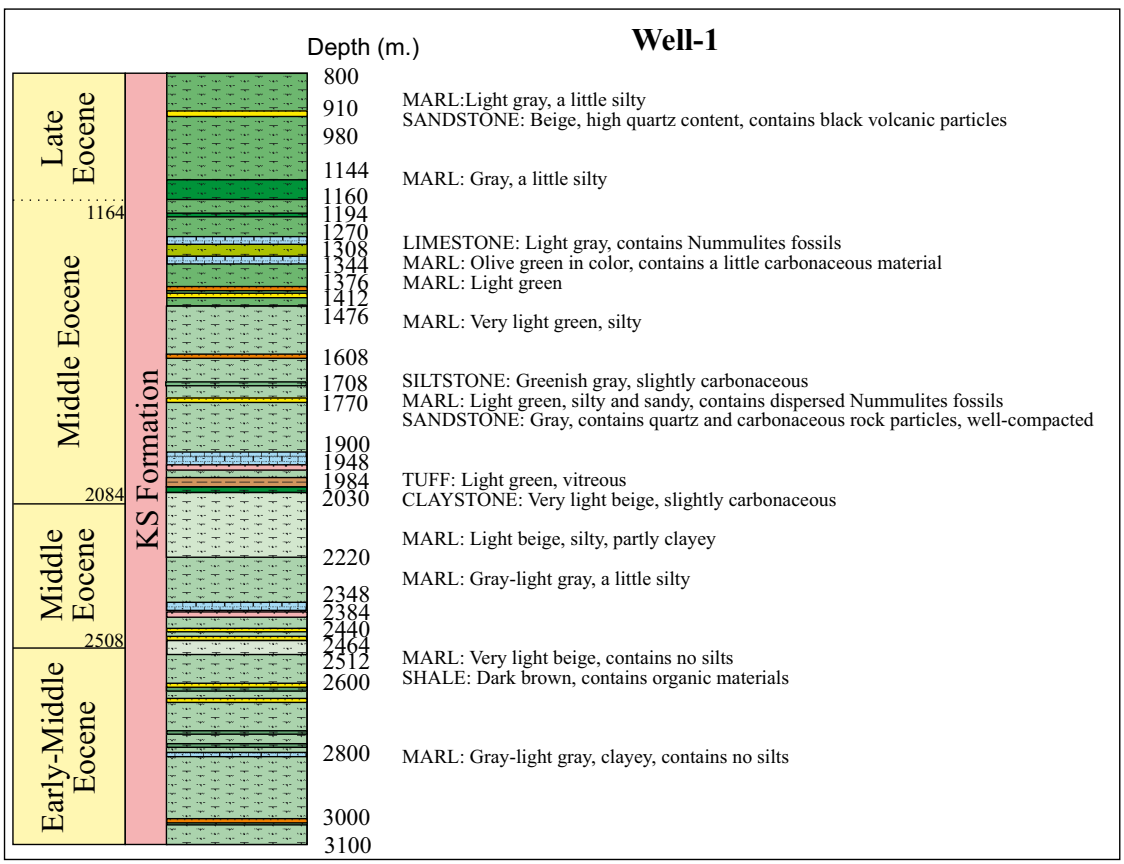

Figure 5. Illustration of columnar section of Well-2 (not to scale).

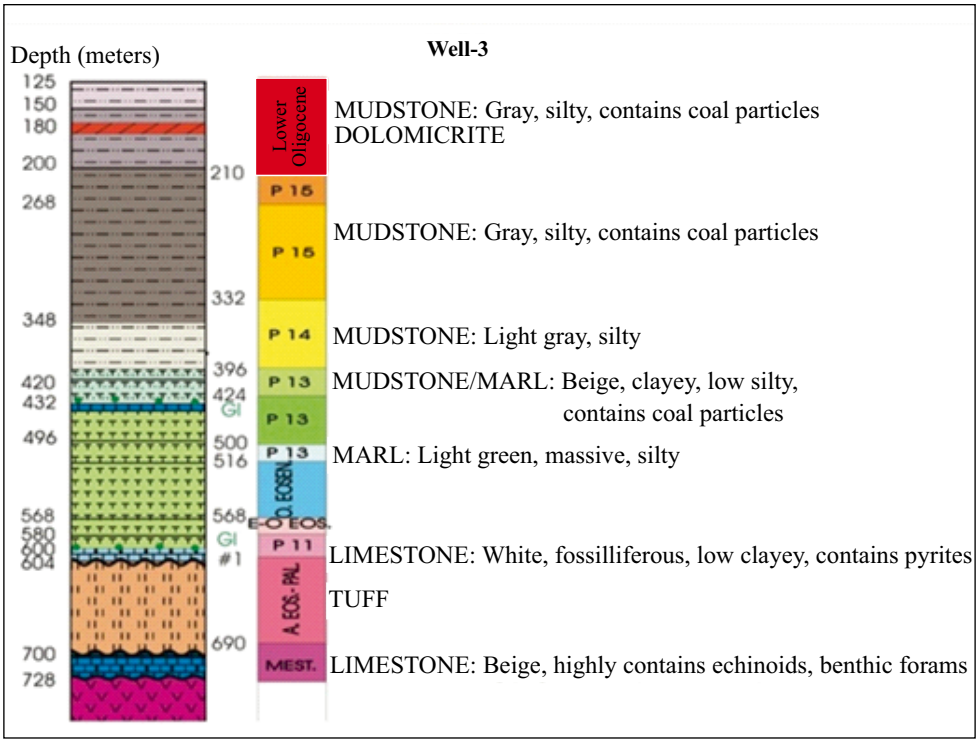

Figure 6. Illustration of columnar section of Well-3 (not to scale).

The key point is the mirror-like changing patterns of smectite and illite amounts. The illite percentage generally increases while the smectite percentage decreases with increasing burial depth. This change suggests that the conversion of smectite to illite takes place in the sedimentary sequences in each well. Two major changes, however, take place in Well-1: the first change is seen after 1400 m depth and the second is seen after 1800 m depth. At the first point, the illite percentage dramatically falls below 10% and the smectite percentage rises above 90%. At the second point, the smectite percentage dramatically falls below 20% and the illite percentage rises above 60%. According to the interpretations, there are two main faults detected at around 1400 m and 1800 m depths. The dramatic changes in clay mineralogy can possibly be explained by the effects of these two main faults (Figure 11).

The chemical results of major oxides acquired from XRF analyses (Table 1) show changes in K_2O, Na_2O, SiO_2, and Al_2O_3 with the increase in burial depth in determination of the conversion of smectite to illite (Figures 12 and 13). The Na_2O and K_2O values, as seen in the graphics, do not gradually increase or decrease. Those kinds of irregular patterns indicate that changes in weight percentages of Na_2O and K_2O values are not simply responsible for the conversion of smectite to illite.

In order to understand the source materials of samples (sediments) of each well, Zr/TiO_2 ratio against depth graphics (Figure 13) and Zr/TiO_2 ratio versus Nb/Y ratio diagrams, which were firstly suggested by Winchester and Floyd (1977), would be helpful (Figure 14). In Well-2 and Well-3, changes in Zr/TiO_2 ratios with increasing depth do not show an important difference (Table 2). The source rock of samples of these two wells is andesite, and so trends in Zr/TiO_2 ratios are reasonable because the sources are composed only of andesitic rocks. In Well-1, the ratio shows different trends and the source rocks of the samples of this well are multiple. This result indicates that samples in the circles in the Zr/TiO_2 against depth graphic of Well-1 are from three different sources. The source rock of the samples in the upper circle is andesite; the source rocks of the samples in the middle circle are trachyandesite and dacite/rhyodacite. The source rock of the samples in the bottom circle is dacite/rhyodacite. Chemical changes in K_2O and Na_2O with increasing burial depth show that the Na_2O percentage is slightly increasing in Well-1 and Well-2, but slightly decreasing in Well-3, and the K_2O percentage shows slight decreasing trends in all the wells. Al_2O_3 percentages are almost constant in Well-1 and Well-2, and there is a slight decrease in Well-3. SiO_2 percentages are slightly decreasing in Well-1 and Well-3 and slightly increasing in Well-2.

The SEM-EDS analyses show that the studied sediment sequence contains some minerals that originated from volcanic rocks. The determination of such minerals like biotite and apatite in SEM analyses is evidence of

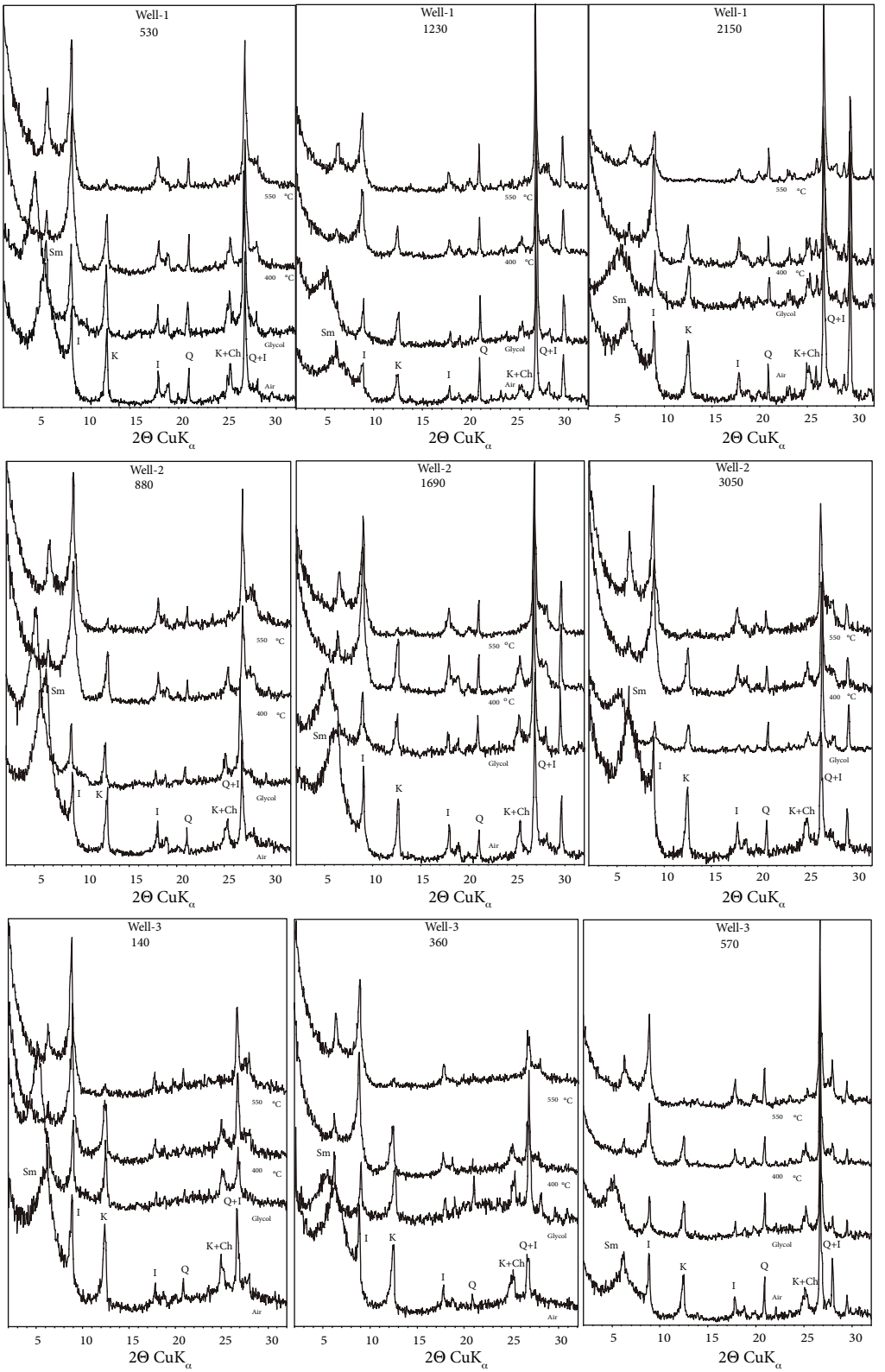

Figure 7. XRD diffractograms of some representative samples (C: Calcite, Ch: Chlorite, I: Illite, K: Kaolinite, Q: Quartz, Sm: Smectite).

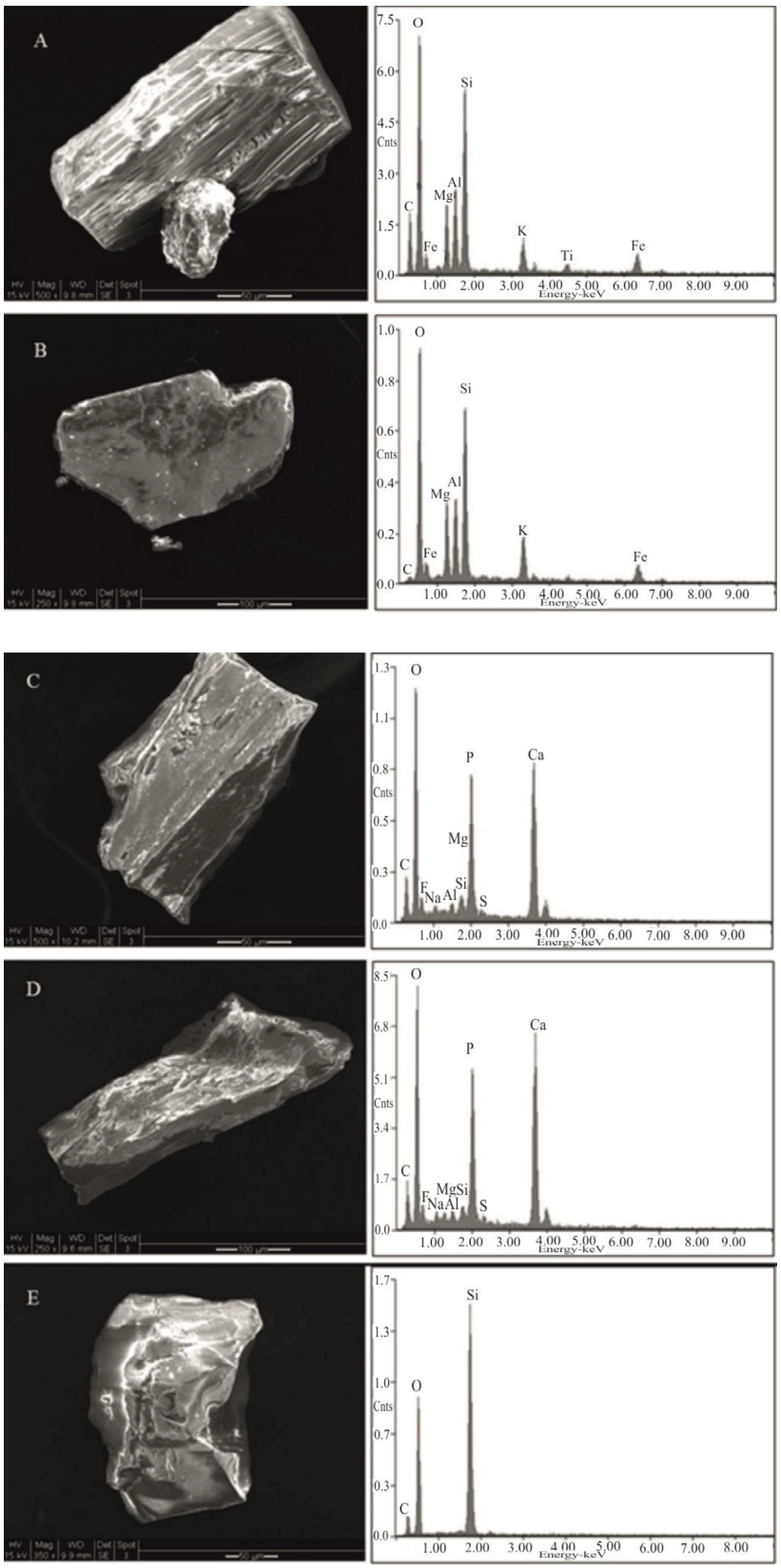

Figure 8. ESEM images and chemistry of some phenocrysts (A and B: Biotite phenocrystals from 570 m depth of Well-3, C: An apatite phenocrystal from 240 m depth of Well-3, D: An apatite phenocrystal from 570 m. of Well-3, E: A quartz phenocrystal from 880 m of Well-2).

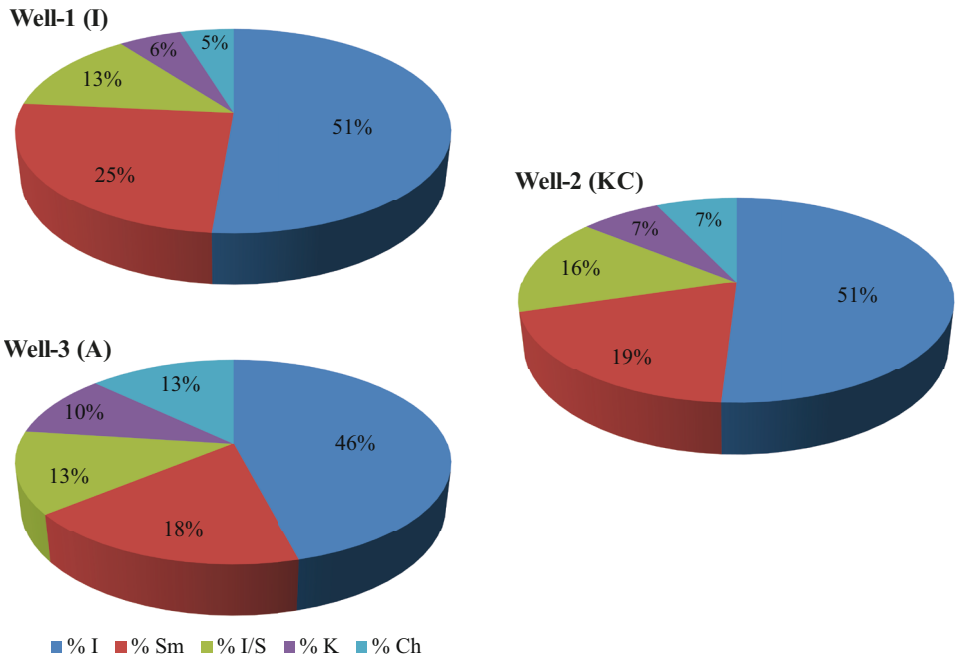

Figure 9. Average clay mineral percentages in each well (I: illite; Sm: smectite; I/S: mixed-layer illite/smectite; K: kaolinite; Ch: chlorite).

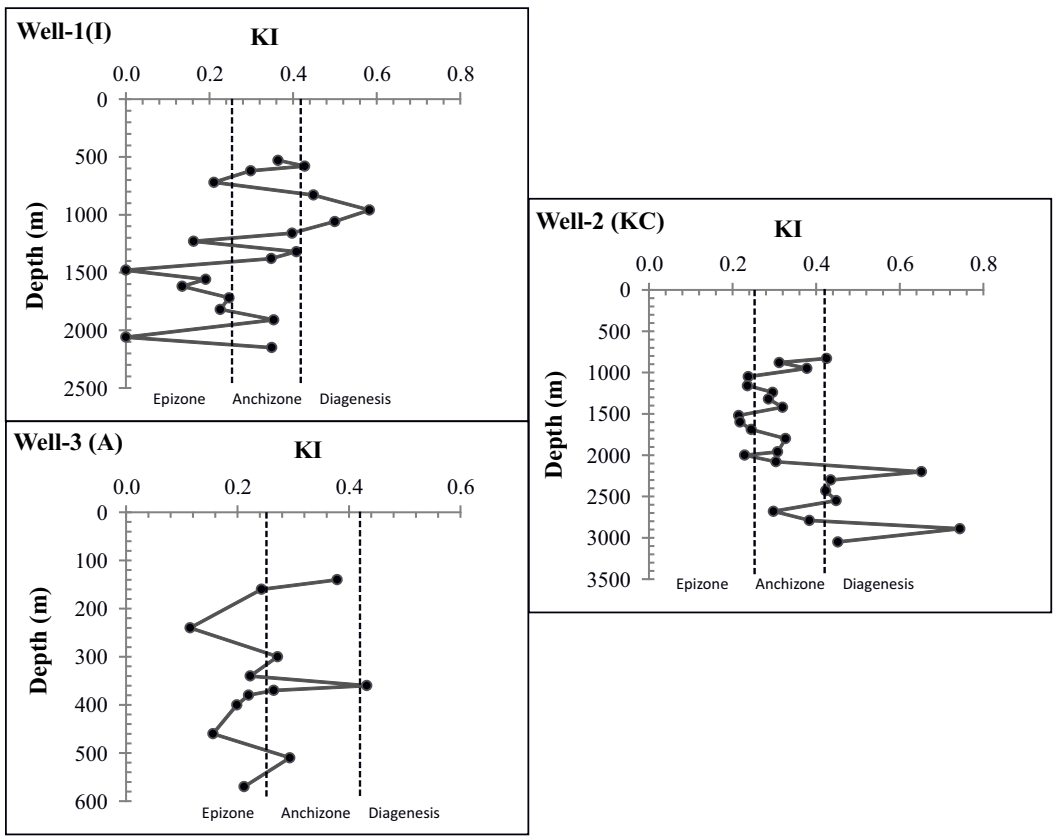

Figure 10. Illite crystallinity (Kübler index) values of the samples against depth graphic (zone boundaries are used from Kübler, 1967).

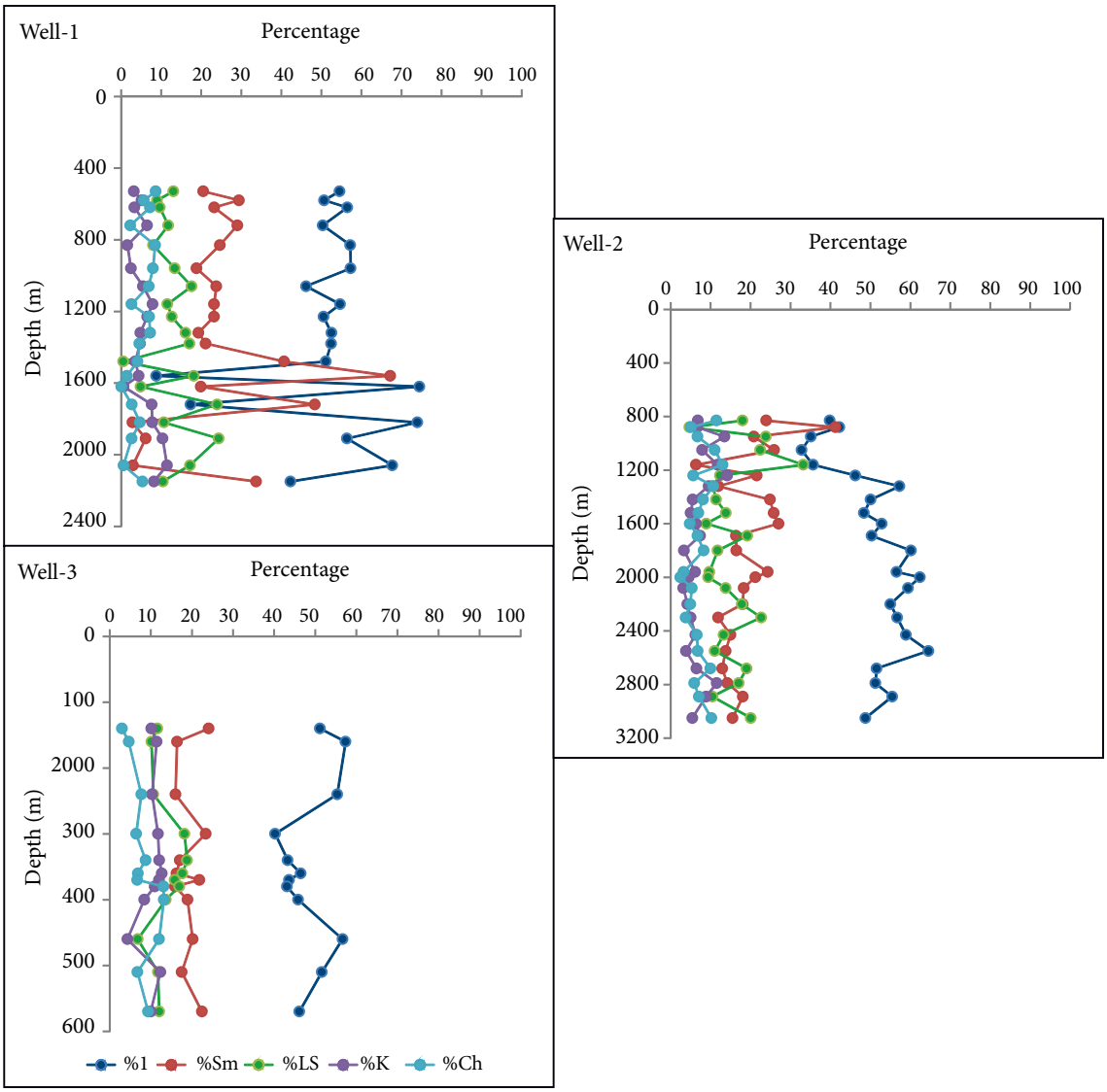

Figure 11. Changes in clay mineral percentages against depth.

transportation of materials that originated from volcanic source rocks into the depositional area. The SEM-EDS analyses are also used for interpreting the source of the detritic clay minerals and the source of possible ash falls that have been deposited in the basin and become a source of smectite in the sediment sequence.

The conversion of smectite to illite becomes possible with the substitution of Na ions by K ions with the increasing of burial depth. According to the early studies by Perry and Hower (1970), Hower et al. (1976), and Pearson and Small (1988), the source of K ion in the system is generally the decomposition of K-feldspars and/or mica minerals, and then the tetrahedral substitution of Al^{+3} for Si^{+4} produces appropriate space for fixing of the K ion. This mechanism, which is explained by Perry and Hower (1970) and Hower et al. (1976), is also known as the diagenetic transformation model. According to Nadeau et al. (1985), there is another mechanism, called the neoformation or dissolution/precipitation model for conversion of smectite to illite crystals. The assumption made here is that the composition in the sedimentary sequence is constant. In other words, the sediments in the depositional environment have come from a single source and the changes in the sequence occur within the depositional area's own dynamics. The K_2O values of the samples in each well do not change very much and so the K^+ concentration has substantially been conserved in the depositional sequence, but has shown minor fluctuation in some depths of each well. Moreover, the addition of the detritic materials commonly from andesitic volcanic

Table 1. XRF results of major oxides (wt%) (values of Well-1 [Well-I]).

Sample depth (m)	SiO_2	TiO_2	Al_2O_3	Fe_2O_3	MnO	MgO	CaO	Na_2O	% K_2O	P_2O_5	LOI
530	45.1	0.60	11.2	4.66	0.07	2.38	13.5	0.47	4.24	0.12	17.9
580	47.1	0.61	11.7	4.70	0.07	2.34	11.4	0.63	4.19	0.12	17.0
620	43.4	0.54	10.2	3.96	0.07	2.05	14.2	0.56	4.96	0.09	19.8
720	44.2	0.54	10.5	4.07	0.07	2.10	13.7	0.63	4.89	0.09	19.1
830	43.0	0.55	10.1	4.17	0.07	2.09	15.1	0.58	4.61	0.10	19.7
960	42.2	0.55	10.3	4.29	0.07	2.19	14.4	0.55	4.93	0.10	20.4
1060	45.4	0.58	10.7	4.41	0.07	2.25	13.4	0.56	4.18	0.12	18.4
1160	43.8	0.53	10.4	4.15	0.08	2.14	13.8	0.58	4.58	0.10	19.7
1230	44.4	0.53	9.8	3.97	0.08	2.08	15.7	0.59	4.09	0.11	18.6
1320	24.7	0.26	7.5	1.96	0.11	1.41	27.9	0.76	3.80	0.13	31.7
1380	23.6	0.25	6.9	1.76	0.06	1.37	29.7	0.60	3.26	0.15	32.5
1480	33.5	0.33	7.3	2.19	0.04	2.11	25.0	0.77	2.55	0.05	26.4
1560	34.8	0.32	8.1	2.19	0.04	1.50	23.6	0.87	2.97	0.05	26.0
1620	41.3	0.41	10.4	2.99	0.03	1.71	17.2	1.99	3.28	0.06	21.6
1720	38.7	0.46	10.6	4.34	0.06	1.51	17.0	0.61	3.96	0.08	21.9
1820	45.5	0.51	10.8	3.44	0.07	1.92	13.8	0.82	3.82	0.08	18.2
1910	37.1	0.38	9.5	2.48	0.07	1.71	19.7	1.07	3.39	0.09	25.0
2060	43.3	0.48	9.7	3.39	0.08	1.88	16.4	0.71	3.51	0.09	19.6
2150	43.2	0.45	10.5	2.93	0.09	1.97	16.6	0.98	3.30	0.09	20.2

Table 1. (Continued). (values of Well-2 [Well-KC]).

Sample depth (m)	SiO_2	TiO_2	Al_2O_3	Fe_2O_3	MnO	MgO	CaO	Na_2O	K_2O	P_2O_5	LOI
830	41.0	0.59	10.59	4.81	0.07	2.57	14.2	0.49	4.96	0.11	20.7
880	39.7	0.56	10.14	4.54	0.07	2.40	15.1	0.49	5.39	0.09	21.6
950	41.5	0.59	10.81	4.56	0.06	2.61	13.3	0.66	5.26	0.10	20.7
1050	40.4	0.57	10.78	4.62	0.07	2.52	14.2	0.61	5.24	0.09	21.0
1160	42.3	0.62	11.24	4.92	0.07	2.73	13.0	0.67	4.91	0.11	19.5
1240	40.7	0.57	12.60	5.80	0.13	2.70	15.3	0.61	3.05	0.06	19.3
1320	36.4	0.54	9.40	4.91	0.10	2.41	18.1	1.52	4.33	0.11	22.1
1420	40.4	0.55	11.07	4.84	0.09	2.45	13.5	1.48	4.94	0.09	20.4
1520	41.7	0.56	10.75	4.73	0.09	2.33	13.8	0.68	4.99	0.10	20.2
1600	42.3	0.57	10.64	4.88	0.09	2.36	14.6	0.71	4.42	0.09	19.5
1690	41.5	0.55	10.23	4.53	0.08	2.24	15.4	0.67	4.54	0.09	20.1

Table 1. (Continued).

1800	45.9	0.60	11.57	4.89	0.12	2.46	11.7	0.76	4.20	0.13	17.5
1960	44.8	0.54	12.60	5.62	0.22	2.13	14.0	0.65	2.45	0.07	16.7
2000	47.1	0.57	12.80	6.06	0.20	2.19	12.3	0.66	2.35	0.08	15.8
2080	44.7	0.54	12.00	5.49	0.08	2.22	12.3	0.74	2.92	0.12	18.7
2200	44.0	0.52	11.40	4.98	0.07	2.15	13.5	0.62	2.75	0.07	19.6
2300	42.7	0.53	11.70	4.99	0.06	2.25	14.7	0.61	2.71	0.07	19.1
2430	44.6	0.57	12.40	5.45	0.08	2.14	11.5	1.08	3.13	0.08	16.0
2550	47.9	0.58	12.90	6.17	0.15	2.28	10.6	0.76	2.84	0.08	15.7
2680	43.7	0.51	11.34	4.72	0.20	2.22	11.0	0.99	4.78	0.14	19.6
2790	48.6	0.60	12.20	5.45	0.18	2.44	9.3	0.66	3.60	0.17	16.4
2890	41.8	0.58	10.89	4.58	0.07	2.52	13.2	0.73	5.26	0.10	20.3
3050	43.1	0.58	10.74	4.65	0.07	2.47	13.7	0.75	4.49	0.12	19.4

Table 1. (Continued). (values of Well-3 [Well-A]).

Sample depth (m)	SiO_2	TiO_2	Al_2O_3	Fe_2O_3	MnO	MgO	CaO	Na_2O	K_2O	P_2O_5	LOI
530	45.1	0.60	11.19	4.66	0.07	2.38	13.5	0.47	4.24	0.12	17.9
580	47.1	0.61	11.74	4.70	0.07	2.34	11.4	0.63	4.19	0.12	17.0
620	43.4	0.54	10.23	3.96	0.07	2.05	14.2	0.56	4.96	0.09	19.8
720	44.2	0.54	10.51	4.07	0.07	2.10	13.7	0.63	4.89	0.09	19.1
830	43.0	0.55	10.06	4.17	0.07	2.09	15.1	0.58	4.61	0.10	19.7
960	42.2	0.55	10.27	4.29	0.07	2.19	14.4	0.55	4.93	0.10	20.4
1060	45.4	0.58	10.71	4.41	0.07	2.25	13.4	0.56	4.18	0.12	18.4
1160	43.8	0.53	10.35	4.15	0.08	2.14	13.8	0.58	4.58	0.10	19.7
1230	44.4	0.53	9.78	3.97	0.08	2.08	15.7	0.59	4.09	0.11	18.5
1320	24.7	0.26	7.47	1.96	0.11	1.41	27.9	0.76	3.80	0.13	31.7
1380	23.6	0.25	6.90	1.76	0.06	1.37	29.7	0.60	3.26	0.15	32.5
1480	33.5	0.33	7.28	2.19	0.04	2.11	25.0	0.77	2.55	0.05	26.4
1560	34.8	0.32	8.07	2.19	0.04	1.50	23.6	0.87	2.97	0.05	26.0
1620	41.3	0.41	10.43	2.99	0.03	1.71	17.2	1.99	3.28	0.06	21.6
1720	38.7	0.46	10.57	4.34	0.06	1.51	17.0	0.61	3.96	0.08	21.9
1820	45.5	0.51	10.76	3.44	0.07	1.92	13.8	0.82	3.82	0.08	18.2
1910	37.1	0.38	9.49	2.48	0.07	1.71	19.7	1.07	3.39	0.09	25.0
2060	43.3	0.48	9.68	3.39	0.08	1.88	16.4	0.71	3.51	0.09	19.6
2150	43.2	0.45	10.53	2.93	0.09	1.97	16.6	0.98	3.30	0.09	20.2

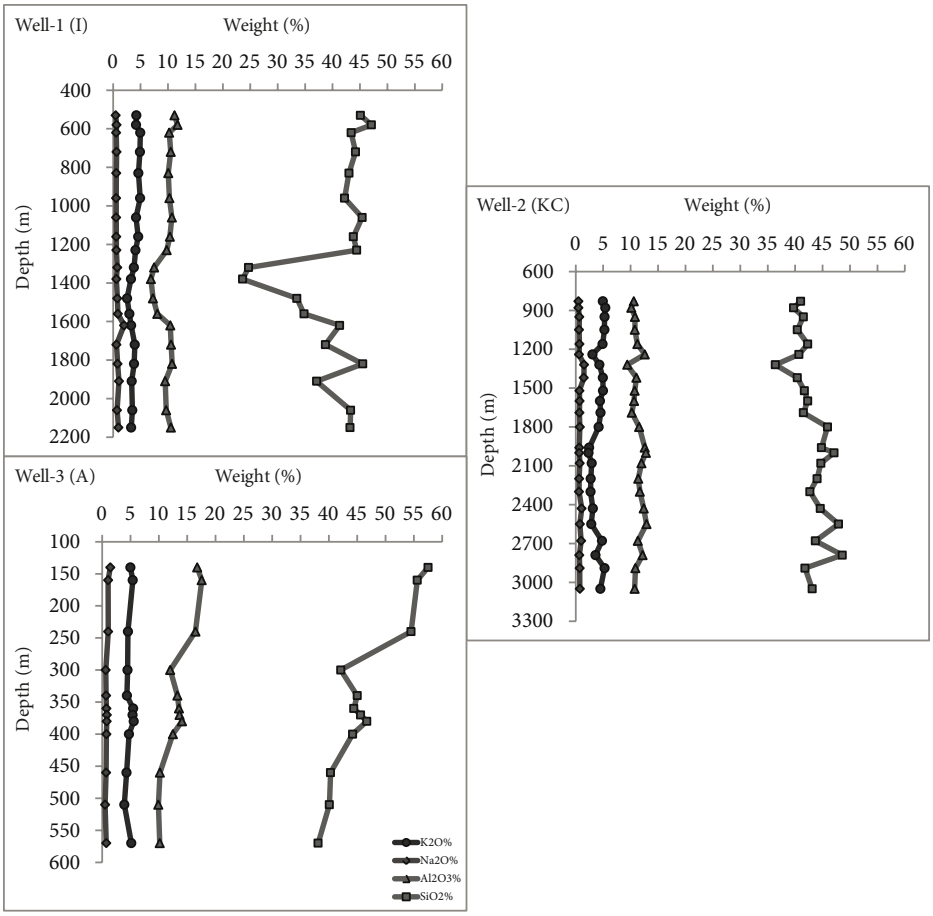

Figure 12. Changes in K_2O, Na_2O, Al_2O_3, and SiO_2 percentages against depth.

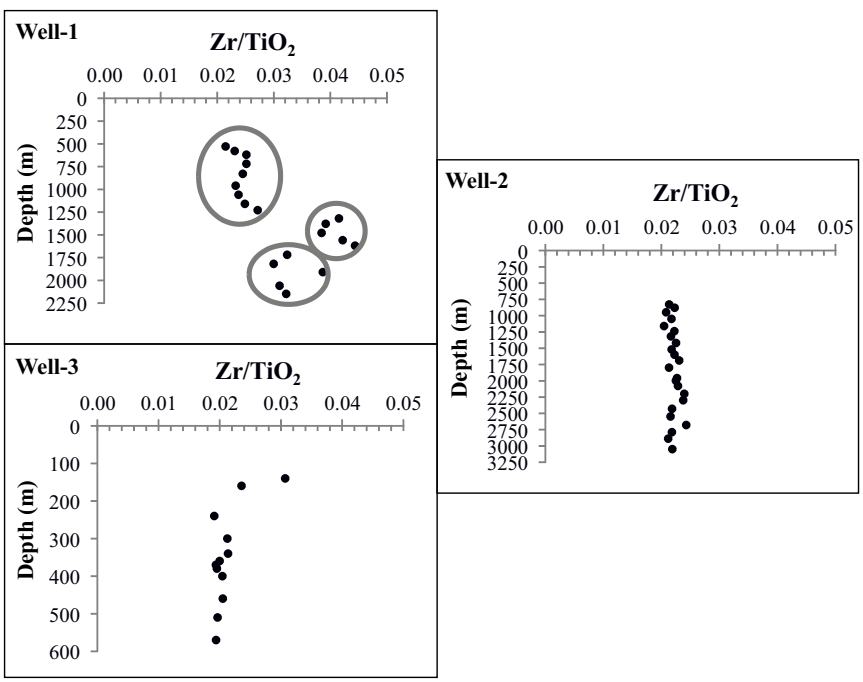

Figure 13. Changes in Zr/TiO_2 ratio against increasing depth in each well.

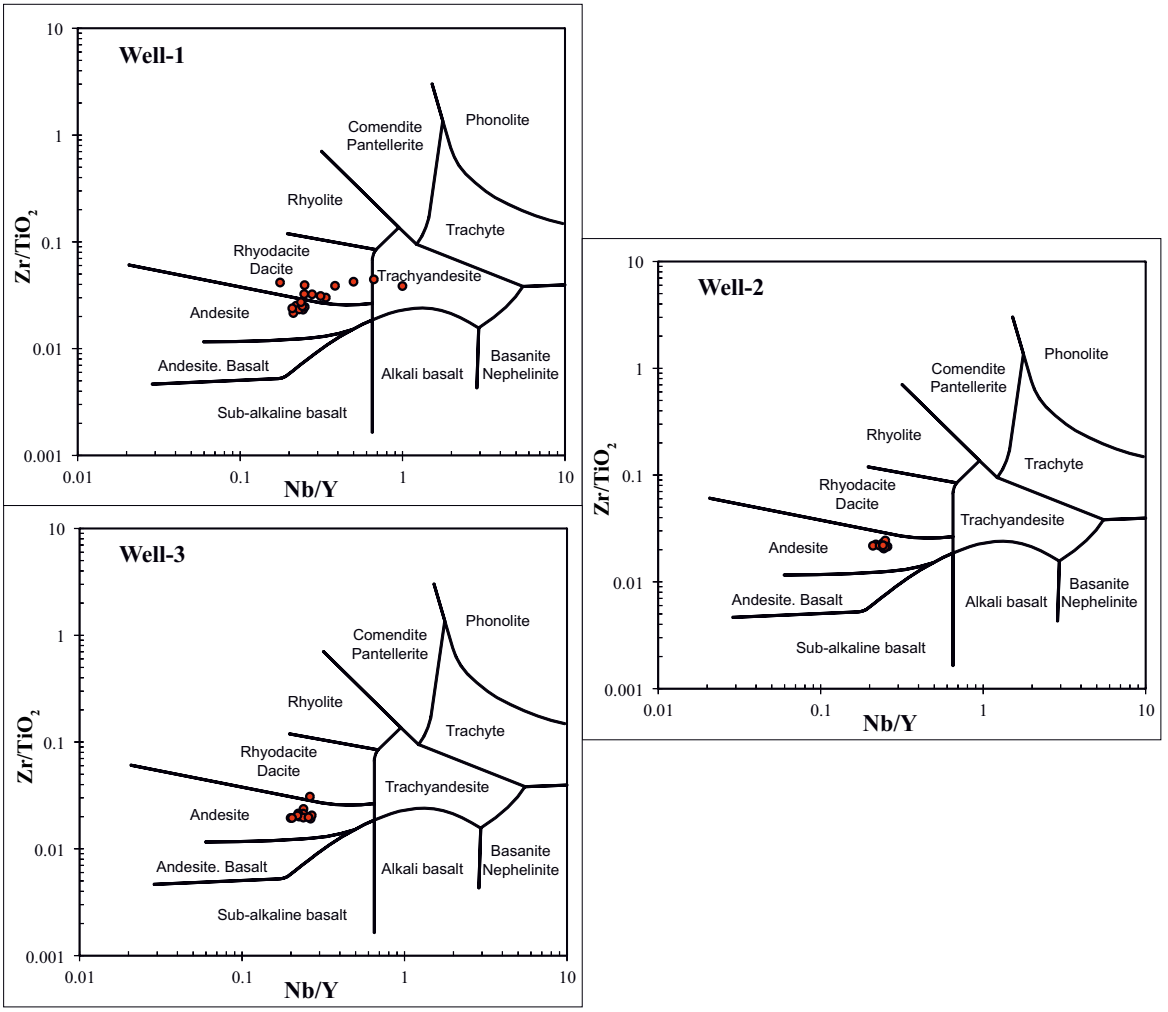

Figure 14. Zr/TiO2 vs. Nb/Y diagrams.

terrestrial source rocks into the depositional area can disrupt the neoformation mechanism and the burial diagenesis becomes a more reasonable explanation for the transformation process of smectite to illite.

According to Velde (1995), the geothermal gradient is about 25–35 °C/km in continental margins, 30–40 °C/km in basins formed in midcontinent regions, and 40–60 °C/km in rift areas. The Black Sea Basin is considered a rift basin (Görür, 1988; Okay, 2008); thus the geothermal gradient in the region can be thought of as about 40–60 °C/km. The maximum sample depths of the wells are 2150 m, 3050 m, and 570 m in Well-1, Well-2, and Well-3, respectively. As a result, the maximum temperature ranges of the conversion of smectite to illite are about 111–154 °C in Well-1, 147–208 °C in Well-2, and 48–59 °C in Well-3. These temperature ranges are for the maximum depths, and it is known that the conversion of smectite to illite can start at shallower depths. Thus, the average temperature ranges for the conversion can be estimated as 56–77 °C in Well-1, 74–104 °C in Well-2, and 24–30 °C in Well-3.

Based on the similarity of the lithologies, changes in clay mineral percentages with depth, and major and trace element chemistries of the samples, a stratigraphic correlation pattern between the three wells is proposed (Figure 15). Lithologies in Well-1 and Well-2 show quite similar characteristics. The bottom sequence (similar lithologic packages) of Well-3 is also similar to the top sections of the other two wells. Chemical fingerprints of that sequence of Well-3, however, do not exactly match similar sequences of the other wells (the changing patterns of K_2O and Na_2O are slightly different from Figure 12 because of using different scales). The sequence, as a suggestion, should be seen somewhere above the uppermost part of Well-2 (blank uncolored section at the top of Well-2). Another explanation should be made for the subsequences seen in purple (the pattern with slashes

Table 2. XRF contents of some trace elements (ppm) on depth.

Well-1				Well-2				Well-3			
Depth (m)	Nb	Y	Zr	Depth (m)	Nb	Y	Zr	Depth (m)	Nb	Y	Zr
530	8.3	39	129	830	8.0	31.0	126	140	14.7	56	212
580	9.5	39	141	880	7.0	32.0	125	160	13.2	55	165
620	8.1	34	136	950	8.0	33.0	123	240	13.2	50	153
720	7.3	33	136	1050	6.9	33.0	124	300	8.8	37	134
830	8.5	34	135	1160	8.3	34.0	127	340	8.9	40	141
960	7.6	33	128	1240	0.0	33.2	127	360	9.0	40	128
1060	7.3	35	138	1320	7.0	29.0	117	370	8.4	42	130
1160	7.8	32	132	1420	8.3	34.0	124	380	9.8	41	129
1230	7.4	31	144	1520	7.6	33.0	122	400	8.8	40	135
1320	3.0	17	108	1600	8.5	35.0	127	460	8.3	31	121
1380	4.0	16	98	1690	8.0	33.0	127	510	8.2	32	114
1480	1.0	1.0	127	1800	9.0	37.0	128	570	6.3	31	101
1560	2.0	4.0	135	1960	0.0	36.0	123				
1620	2.0	3.0	182	2000	0.0	38.5	128				
1720	1.7	7.0	149	2080	0.0	34.3	124				
1820	5.4	16	153	2200	0.0	32.2	125				
1910	5.0	13	147	2300	0.0	33.2	126				
2060	5.0	16	149	2430	0.0	35.6	125				
2150	5.0	18	145	2550	0.0	38.4	125				
				2680	9.0	36.0	124				
				2790	10.0	41.0	131				
				2890	8.0	32.0	123				
				3050	8.0	33.0	127				

showing the marl lithology light beige, silty, and partly clayey) in Well-1 and Well-2. Although the lithologies (marl units with different features) are the same, chemical fingerprints and clay mineral percentages do not clearly match those purple subsequences and so a question mark has been put in the area instead of correlation dash lines.

5. Conclusions

Illite is the most dominant clay mineral in each well, and smectite follows it. The mixed-layer I/S phase also exists but is not dominant. The co-occurrence of discrete illite with I/S and the recessive character of I/S are not common and this condition is very attractive. The existence of the individual illite of detritic origin and mixed layer I/S of diagenetic origin together shows that detritic clayey materials have been transported to the depositional area during the burial diagenesis (or neoformation).

Analyzing the characters of detritic and diagenetic types of illite and smectite in the wells shows that the amount of illite increases with the increasing burial depth while the amount of smectite decreases in the three wells. The mirror-shaped changes in the amounts of illite and smectite suggest that the conversion of smectite to illite takes place in the sedimentary sequences in each well; however, the mechanism of the conversions is not obvious because of the conserved amount of K_2O values in the wells with minor fluctuations and the presence of detritic and diagenetic forms of illite together.

K_2O and Na_2O weight percentage trends do not show a linear relationship with increasing depth. Al_2O_3 and SiO_2 weight percentages do not show a linear relationship either. These results suggest that volcanism affected the region. The source rocks of the samples of all wells are mainly from andesitic volcanic rocks. On the other hand, some

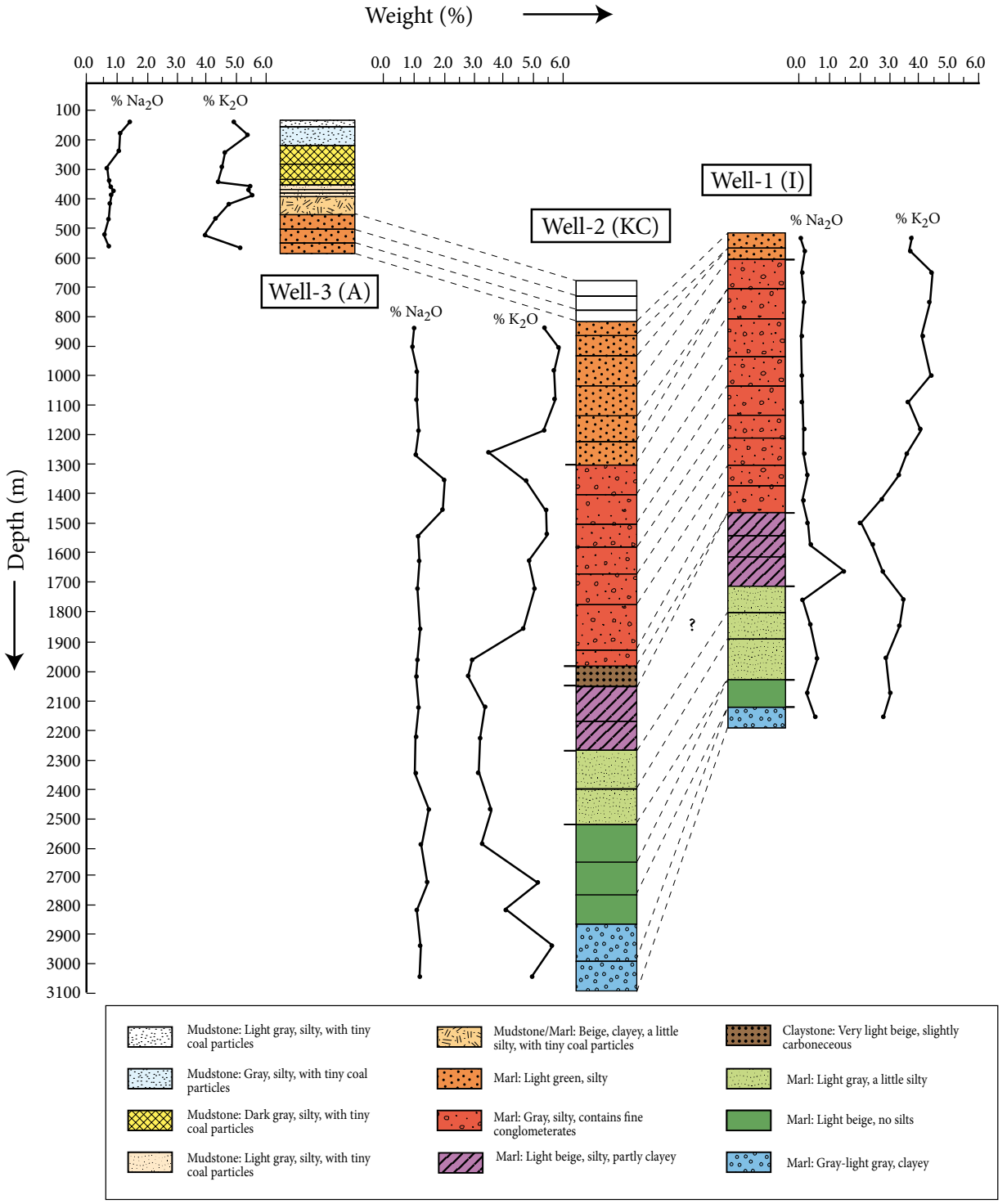

Figure 15. Suggested stratigraphic correlation pattern for the three wells. (The changing patterns of K_2O and Na_2O are seen slightly different from Figure 12 because of using different scales.).

of the samples of Well-1 are from two different volcanic source rocks as rhyodacitic/dacitic and trachyandesitic rocks. These results are also supported by the SEM-EDS analyses, which have made it possible to determine some volcanic minerals such as biotite and apatite in the studied sediment sections, and supported by Zr/TiO_2 ratio against

depth graphics. These types of volcanic rocks may also be the origin of detrital clays that have been transported to the study area.

As a prediction, the minimum and maximum temperature ranges of the conversion of smectite to illite are approximately 111–154 °C in Well-1, 147–208 °C in Well-2, and 48–59 °C in Well-3; and the average temperature ranges are 56–77 °C in Well-1, 74–104 °C in Well-2, and 24–30 °C in Well-3. These temperature ranges have been calculated by the geothermal gradient values as explained in Velde (1995). Wide temperature ranges between the first two wells and Well-3 are caused by the great differences in depths between the studied sections of the wells.

Acknowledgments

The authors thank Tammie L Gerke and J Barry Maynard, who completed and corrected the XRF analyses, and Attila I Kilinc for comments and suggestions. The Turkish Petroleum Corporation Research Center is thanked for providing the samples and financial support.

References

Burst JF (1959). Postdiagenetic clay mineral environmental relationships in the Gulf Coast Eocene. Clay Clay Miner 6: 327-341.

Chen F, Siebel W, Satir M, Terzioğlu N, Saka K (2002). Geochronology of the Karadere basement (NW Turkey) and implications for the geological evolution of the İstanbul Zone. Int J Earth Sci 91: 469-481.

Drits VA, Lindgren H, Sakharov BA, Jakobsen HJ, Salyn AL, Dainyak LG (2002). Tobelitization of smectite during oil generation in oil-source shales: application to North Sea illite-tobelite-smectite-vermiculite. Clay Clay Miner 50: 82-98.

Dunoyer de Segonzac G (1964). Les Argiles du Cretace Superior dans le bassin de Douala (Cameroun): Problems de diagenese. Alsace-Lorraine Service Carte Geologie Bulletin 17: 287-310.

Fowler AC, Yang XS (2003). Dissolution/precipitation mechanism for diagenesis in sedimentary basins. J Geophys Res 108 (B10): 2509.

Freed RL, Peacor DR (1992). Diagenesis and the formation of authigenic illite-rich I/S crystals in Gulf Coast shales: TEM study of clay separates. J Sediment Petrol 62: 220-234.

Görür N (1988). Timing of opening of the Black Sea basin. Tectonophysics 147: 247-262.

Hamilton PJ, Kelley S, Fallcik AE (1989). K-Ar dating of illite in hydrocarbon reservoirs. Clay Miner 24: 215-231.

Hoffman J, Hower J (1979). Clay mineral assemblages as low grade metamorphic geothermometers: application to the thrust faulted disturbed belt of Montana, in Aspects of Diagenesis. In: Scholle PA, Schluger PS, editors. SEPM Special Publications 26: pp. 56-79.

Hower J, Eslinger EV, Hower ME, Perry EA (1976). Mechanism of burial metamorphism of argillaceous sediment: mineralogical and chemical evidence. Geol Soc Am Bull 87: 725-737.

Jaboyedoff M, Bussy F, Kübler B, Thelin P. (2001). Illite "crystallinity" revisited. Clay Clay Miner 49: 156-167.

Jiang S (2012). Clay minerals from the perspective of oil and gas exploration. In: Valaskova M, Martynkova GS, editors. Clay Minerals in Nature - Their Characterization, Modification and Application. 1st ed. Rijeka, Croatia: InTech, pp. 21-38.

Kelly J, Parnell J, Chen HH (2000). Application of fluid inclusions to studies of fractured sandstone reservoirs. J Geochem Explor 69: 705-709.

Kübler B (1967). La cristallinité de l'illite et les zones tout à fait supérieures du métamorphisme. In: Etages tectoniques, Colloque de Neuchâtel 1966, Edition de la Baconniére. Neuchâtel, Switzerland: 105-121.

Liewig N, Clauer N, Sommer F (1987). Rb-Sr and K-Ar dating of clay diagenesis in Jurassic sandstone oil reservoir, North Sea. AAPG Bull 71: 1467-1474.

Moore DM, Reynolds RC (1997). X-Ray Diffraction and the Identification and Analysis of Clay Minerals. 2nd ed. New York, NY, USA: Oxford University Press.

Nadeau PH, Wilson MJ, McHardy WJ, Tait JM (1985). The conversion of smectite to illite during diagenesis: evidence from some illitic clays from bentonites and sandstones. Mineral Mag 49: 393-400.

Okay AI (2008). Geology of Turkey: a synopsis. Anschnitt 21: 19-42.

Okay AI, Tüysüz O (1999). Tethyan sutures of northern Turkey. In: Durand B, Jolive L, Horvath F and Serrane M, editors. The Mediterranean Basins: Tertiary Extensions within Alpine Orogen. 1st ed. London, UK: Geological Society Special Publications 156, pp. 475-515.

Okay AI, Şengör AMC, Görür N (1994). Kinematic history of the opening of the Black Sea and its effect on the surrounding regions. Geology 22: 247-270.

Okay AI, Satır M, Maluski H, Siyako M, Monie P, Metzger R, Akyüz S (1996). Paleao- and neo-Tethyan events in northwestern Turkey: geologic and geochronologic constrains. In: Yin A, Harrison TM editors. The Tectonic Evolution of Asia. 1st ed. London, UK: Cambridge University Press, pp. 420-441.

Pearson MJ, Small JS (1988). Illite/smectite diagenesis and palaeotemperatures in Northern North Sea Quaternary to Mesozoic shale sequences. Clay Miner 23: 109-132.

Perry E, Hower J (1970). Burial diagenesis in Gulf Coast pelitic sediments. Clay Clay Miner 18: 165-177.

Underwood MB, Pickering KT (1996). Clay-mineral provenance, sediment dispersal patterns, and mudrock diagenesis in the Nankai Accretionary Prism, Southwest Japan. Clay Clay Miner 44: 339-356.

Ustaömer PA, Mundil R, Renne PR (2005). U/Pb and Pb/Pb zircon ages for arc-related intrusions of the Bolu Massif (W Pontides, NW Turkey): evidence for Late Precambrian (Cadomian) age. Terra Nova 17: 215-223.

Velde B (editor) (1995). Origin and Mineralogy of Clays: Clays and the Environment. 1st ed. Heidelberg, Germany: Springer.

Weaver CE (1958). Geologic interpretation of argillaceous sediments. AAPG Bull 42: 254-309.

Weaver CE (1960). Possible uses of clay minerals in search for oil. AAPG Bull 44: 1505-1518.

Winchester JA, Floyd PA (1977). Geochemical discrimination of different magma series and their differentiation products using immobile elements. Chem Geol 20: 325-343.

Yariv S (1976). Organophilic pores as proposed primary migration media for hydrocarbons in argillaceous rocks. Clay Sci 5: 19-29.

Yiğitbaş E, Kerrich R, Yilmaz Y, Elmas A, Xie QL (2004). Characteristics and geochemistry of Precambrian ophiolites and related volcanics from the İstanbul-Zonguldak Unit, Northwestern Anatolia, Turkey: following the missing chain of the Precambrian South European suture zone to the east. Precambrian Res 132: 179-206.

Yilmaz Y, Tüysüz O, Yiğitbaş E, Genç ŞC, Şengör AMC (1997). Geology and tectonic evolution of the Pontides. In: Robinson AG, editors. Regional and Petroleum Geology of the Black Sea and Surrounding Region. 1st ed. Tulsa, OK, USA: AAPG Memoir 68: pp. 183-226.